

Article

Biological Synthesis and Characterization of Silver-Doped Nanocomposites: Antibacterial and Mechanistic Studies

Franklin Loic Tchinda Taghu ¹, Boniface Pone Kamdem ^{1,2}, Vincent Ngouana ³, Zuriatou Yajeh Tanka ¹,
Victorine Lorette Yimgang ¹, Julius Nsami Ndi ^{4,*}, Paul Keilah Lunga ^{1,*} and Fabrice Fekam Boyom ¹

- ¹ Laboratory for Phytobiochemistry and Medicinal Plants Studies, Antimicrobial and Biocontrol Agents Unit (AmBcAU), Department of Biochemistry, Faculty of Science, University of Yaoundé I, Yaounde P.O. Box 812, Cameroon; ponekamdemboniface@gmail.com (B.P.K.); zuriayajeh@gmail.com (Z.Y.T.); fabrice.boyom@fulbrightmail.org (F.F.B.)
- ² Higher Institute of Agriculture, Forestry, Water and Environment (HIAFW), University of Ebolowa, Ebolowa P.O. Box 755, Cameroon
- ³ Department of Pharmacy, Faculty of Medicine and Pharmaceutical Sciences, University of Dschang, Dschang P.O. Box 96, Cameroon
- ⁴ Applied Physical and Analytical Chemistry Laboratory, Department of Inorganic Chemistry, Faculty of Science, University of Yaounde I, Yaounde P.O. Box 812, Cameroon
- * Correspondence: ndinsami2002@gmail.com (J.N.N.); lungapaul@yahoo.ca (P.K.L.);
Tel.: +237-67-780-7132 (J.N.N.); +237-67-246-0130 (P.K.L.)

Abstract: The development of antimicrobial resistance has increased the prevalence of infectious diseases, causing a global health problem that accounts for over 4.95 million deaths worldwide annually. The side effects associated with current antibiotics prompt a crucial need to search for effective and safe antimicrobial agents. In this study, silver nanoparticles (AgNPs) were prepared by chemical reduction method using silver nitrates as a metallic precursor and *Croton macrostachyus* bark aqueous extract as a reducing and capping agent. The nanoparticles were further functionalized using *C. macrostachyus*-based activated carbon (CAC) to generate nanocomposites (CAC-AgNPs). The nanomaterials were characterized by ultraviolet-visible (UV-vis) absorption spectra and Fourier transform infrared (FTIR) spectra. The antibacterial activity of the as-prepared nanomaterials was evaluated against an array of bacterial strains by microdilution method, whereas their cytotoxicity profile was evaluated using Vero cells (human mammalian cells). Antibacterial mechanistic studies of active nanomaterials were carried out through bacterial growth kinetics, nucleic acid leakage tests, and catalase inhibition assays. As a result, the as-prepared nanomaterials exhibited antibacterial activity against an array of bacterial strains (minimum inhibitory concentration (MIC) range: 62.5 to 500 µg/mL), the most susceptible being *Escherichia coli* and *Staphylococcus aureus*. Cytotoxicity studies of the nanomaterials on Vero cells revealed that the nanocomposite (median cytotoxic concentration (CC₅₀): 213.6 µg/mL) was less toxic than its nanoparticle (CC₅₀ value: 164.75 µg/mL) counterpart. Antibacterial mechanistic studies revealed that the nanomaterials induced (i) bacteriostatic activity vis à vis *E. coli* and *S. aureus* and (ii) inhibition of catalase in these bacteria. This novel contribution regarding the antibacterial mechanisms of action of silver nanocomposites from *C. macrostachyus*-based activated carbon may contribute to our understanding of the antibacterial action of these biomaterials. Nevertheless, more chemistry and in vivo experiments as well as in depth antibacterial mechanistic studies are warranted for the successful utilization of these antibacterial biomaterials.



Citation: Tchinda Taghu, F.L.; Pone Kamdem, B.; Ngouana, V.; Yajeh Tanka, Z.; Yimgang, V.L.; Nsami Ndi, J.; Keilah Lunga, P.; Fekam Boyom, F. Biological Synthesis and Characterization of Silver-Doped Nanocomposites: Antibacterial and Mechanistic Studies. *Drugs Drug Candidates* **2024**, *3*, 13–32. <https://doi.org/10.3390/ddc3010002>

Academic Editor: Jean Jacques Vanden Eynde

Received: 24 October 2023
Revised: 10 December 2023
Accepted: 20 December 2023
Published: 26 December 2023



Copyright: © 2023 by the authors. Licensee MDPI, Basel, Switzerland. This article is an open access article distributed under the terms and conditions of the Creative Commons Attribution (CC BY) license (<https://creativecommons.org/licenses/by/4.0/>).

Keywords: silver nanomaterials; activated carbon; infectious diseases; antibacterial mechanism of action; cytotoxicity

1. Introduction

Diseases that spread from one person to another and are caused by bacteria, parasites, fungi, and viruses are termed as infectious diseases [1]. Notably, infectious diseases are

also transmitted through bug bites; contaminated food, water, and soil; as well as poor sanitation [2]. Common infectious diseases include the common cold, flu (influenza), stomach flu (gastroenteritis), hepatitis, respiratory syncytial virus (RSV), and COVID 19 [2]. Infectious diseases have a myriad of symptoms or manifestations that may lead to death, if the illnesses in question are left untreated. Infectious diseases are one of the significant causes of morbidity and mortality across the world. Generally, antibiotics are used to diagnose, treat, or prevent bacterial infections; however, mutations resulting from their use may cause bacterial drug resistance [3]. Remarkably, bacteria have seemingly won the battle against antibiotics, since most of them have become resistant to these drugs [4]. It is important to mention that various antimicrobial agents interfere with (i) the synthesis of cell walls, (ii) ribosomal function, (iii) folate synthesis, (iv) biofilm formation, and (v) nucleic acid synthesis [5–9]. Resistance occurs when there are profound modifications to one of these functions. For instance, bacterial resistance to β -lactam antibiotics includes modification of porins (cell-wall proteins) and targets, production of inactivating enzymes, namely beta-lactamases, and autolytic enzymes inactivation [10]. Inhibition of nucleic acid synthesis is observed with quinolones and fluoroquinolones that target DNA synthesis through inhibition of type 2 topoisomerases, such as DNA gyrase and topoisomerase IV [11]. Sulfonamides such as trimethoprim, which are widely used to treat urinary tract infections and pneumonia, bind to dihydrofolate reductase to inhibit the synthesis of folic acid [12]. In addition, ribosomal function is affected by macrolide antibiotics [13]. Aminoglycosides and quinolones have been shown to inhibit biofilm formation by *Pseudomonas aeruginosa* [14,15]. These bacterial drug resistance events, combined with the problem of toxicity as well as the high cost and unavailability of modern therapies justify the crucial need to search for new and safe antimicrobials. Infectious diseases cause over 4.8% of mortalities and an economic loss of more than USD 100 trillion per year worldwide [16]. Since their introduction into health care and clinical practice in the early 20th century starting with the discovery of penicillin in 1928, antibiotics have revolutionized medicine; many of them have been either isolated from natural products or chemically synthesized, and numerous lives have been saved [17]. It is noted that these drugs are increasingly being threatened by bacteria that develop a wide variety of resistance mechanisms. Medicinal plants remain the most abundant natural source of active drugs and are invaluable in the traditional treatment of a number of infectious diseases since time immemorial [18,19]. In fact, medicinal plants have been reported to contain numerous secondary metabolites, including terpenoids, flavonoids, phenolic compounds, alkaloids, tannins, saponins, among others. These metabolites have been reported to inhibit the growth of several microorganisms, including bacteria (*Staphylococcus aureus*, *Escherichia coli*, *Pseudomonas aeruginosa*, *Shigella* spp., etc.).

However, the incorporation of these plant secondary metabolites into nanosized particles has been proven more valuable as this nanosize form can overcome biological barriers and augment the delivery of active principles to the target site, thereby increasing their efficacy [20,21]. Undoubtedly, one of the latest approaches to combat resistant microorganisms include the use of nanotechnology-based antimicrobials [22,23]. Because of the non-specific mechanistic action of metal-based nanoparticles on bacteria, the development of resistance by these microorganisms is difficult. Thus, resistance to antibiotics is not relevant to nanoparticles (NPs) as there is direct contact with the bacterial cell wall without the need to penetrate into microbial cells [23]. Nanoparticles are spherical particles (size: 1–100 nm) that exhibit unique properties due to their high surface area-to-volume ratio. They can be classified into fullerenes and metal, ceramic, and polymeric NPs [24]. In addition, nanoparticles are bioactive products that are stable, dispersed, biocompatible, and affordable [25]. Dakal et al. [26] revealed that silver nanoparticles are able to adhere to the surfaces of cell walls or cell membranes, penetrate inside the cell, and damage organelles such as ribosomes, mitochondria and vacuoles by releasing free ions to produce reactive oxygen species (ROS) [26,27]. The metal used for the fabrication of nanoparticles undergo a reaction with the chemical groups of components of the cell membrane (phosphorus

and sulfur groups) such as proteins, lipids, and DNA bases to generate potential reactive oxygen species [28]. It has been reported that the accumulation of nanoparticles within bacterial cell walls and membranes can induce morphological changes in the bacteria. These include membrane detachment and disruption, shrinkage of cytoplasm, and formation of electron-dense holes [17]. Other reports have highlighted the involvement of the shape and size of nanoparticles as the main factors driving antimicrobial action, with triangular and smaller nanoparticles being the most effective [29]. According to some previously published papers, silver nanoplates possess higher antibacterial action than their silver nanorod or nanosphere counterparts; however, other scientists support a different opinion [30]. The preparation of nanocomposites using activated carbon contributes to increasing the antibacterial action of these products. Because of their light weight, high specific surface area, and favorable electrical and mechanical properties, nanocarbons have recently gained considerable attention [31]. In fact, activated carbon is a porous material with amphoteric characteristics, which is used for the adsorption of organic and inorganic compounds [32]. The high content of oxygen on the surface of activated carbons is crucial for effective adsorption of bacteria, such as *S. aureus* and *E. coli* [33]. Parameters, such as pore size distribution, surface area, pH, and elemental analysis are used to characterize active carbon products [33,34]. Recent studies have demonstrated that activated carbon-supported metal nanoparticles, prepared from plant (*Cassia roxburghii*, *Aloe vera* and *Cinnamomum verum*) extracts, can yield nanocomposites with superior antibacterial efficiency [35–37]. The literature also provides evidence of the use of nanoparticles to develop composites with antimicrobial efficacy [38].

Based on the foregoing considerations, the present study aims to use *Croton macrostachyus* (a plant employed in the traditional treatment of a number of infectious diseases, including malaria and venereal diseases, among others) for the fabrication of carbon-activated immobilized metal nanoparticles. Moreover, antibacterial screening of the fabricated nanocomposite and potential mechanistic bases for antimicrobial action are investigated.

2. Results and Discussion

2.1. Physical and UV–Vis Analysis of the Nanoparticles

Green synthesis of silver nanoparticles was successfully achieved using an aqueous extract of *C. macrostachyus* stem bark along with a solution of silver nitrate (AgNO_3). The change in color observed from pale yellow to dark brown indicated the formation of nanoparticles (Figure 1). The fabrication of AgNPs was further confirmed by UV–vis visible spectroscopy in a wavelength range of 350–900 nm, as described in Figure 2. On the spectra of AgNPs, a spectrophotometric absorption peak was observed at a characteristic wavelength of 443 nm and was attributed to the surface plasmon resonance of the formed nanoparticles. Meanwhile, the spectra of the silver salt and aqueous extract solutions of *C. macrostachyus* showed no peaks. For silver nanoparticles, the λ_{max} values were obtained in the wavelength range of the visible spectrum (400–500 nm) [39]. These results are consistent with a number of studies published on the synthesis of nanomaterials from other plants in which wavelength values corresponding to the visible spectrum were observed for aqueous extracts of *C. sparsiflorus* (457 nm; Kathiravan et al. [40]) and *C. bonplandianum* (415 nm; Kapoor [41]).

In response to challenges (pollution, large energy consumption, and toxicity) associated with wet chemical fabrication of nanomaterials [42], green synthesis, which uses plants such as *Croton macrostachyus* instead of chemical agents to reduce metal ions, is more beneficial because it decreases environmental pollution and toxicity and is inexpensive.



Figure 1. Pictorial representation of the procedure for the green synthesis of silver nanoparticles and nanocomposites from *Croton macrostachyus* stem bark.

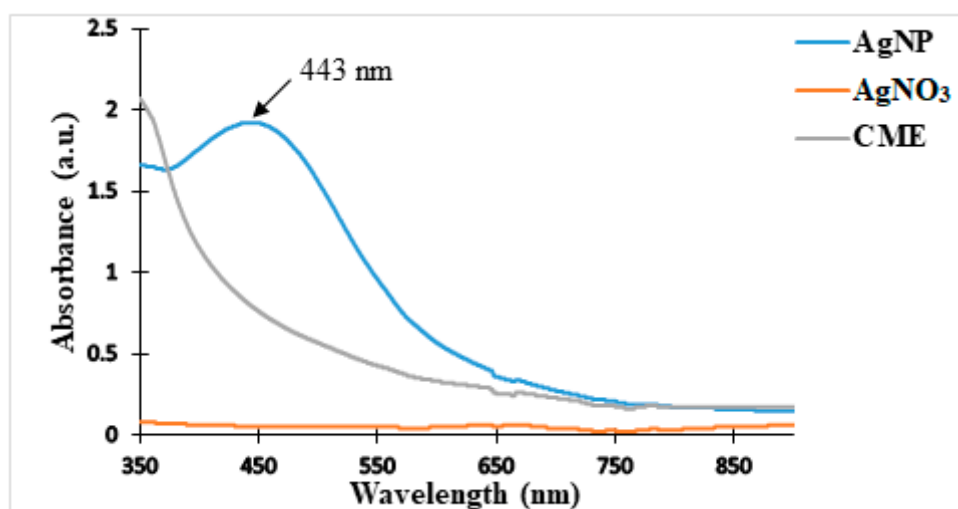


Figure 2. UV-Vis spectra of *C. macrostachyus* extract (CME) compared to those of nanoparticles (AgNP) and the chemical reagent (AgNO_3). AgNO_3 = chemical reagent (silver nitrate); AgNP = silver nanoparticle; CME = *Croton macrostachyus* extract.

2.2. FTIR Analysis of *C. macrostachyus* Extract and Nanoparticles

To identify the plausible functional groups that are involved in the reduction of silver ion to AgNPs, FTIR spectroscopy was performed on the as-prepared extract (*C. macrostachyus* extract) and nanoparticles (AgNPs). The FTIR spectrum (Figure 3) of the aqueous extract of *C. macrostachyus* (blue color) shows a peak at 511 cm^{-1} , which corresponds to the band of alkyl halides. The distortion observed at 781 cm^{-1} may be related to the $\text{CH}=\text{CH}$ bonds of the benzylic aromatic ring of phenols, whereas the presence of an intense peak at 1021 cm^{-1} is characteristic of an aliphatic amine (C-N). At 1304 cm^{-1} , a weak peak, which is characteristic of C-OH groups is observed, whilst another intense peak that corresponds to the C=O groups of protein amides is detected. Moreover, two distinct peaks, which were identified at 2912 cm^{-1} and 3287 cm^{-1} , are potentially linked to the symmetrical elongation vibrations of the $\text{CH}_2\text{-CH}_3$ group of an alkane and the O-H bonds linked to alcohols and phenolic compounds, respectively. These chemical groups are well known to exist in plant extracts as evidenced by previously published research papers [43–45]. The FTIR spectrum (orange color) of AgNPs revealed major peaks at wavelengths of 3300 cm^{-1} (OH bond stretching) and 1634 cm^{-1} (carbonyl C=O group), which correspond to the involvement of hydroxyl and carboxylic acid moieties (encountered in polyphenols, phenolic acids and proteins) of *C. macrostachyus* extract in the reduction of the silver ions (Ag^+). Notably, primary (proteins) and secondary (polyphenols) metabolites are responsible for the formation and stabilization of silver nanoparticles (AgNPs) [46,47].

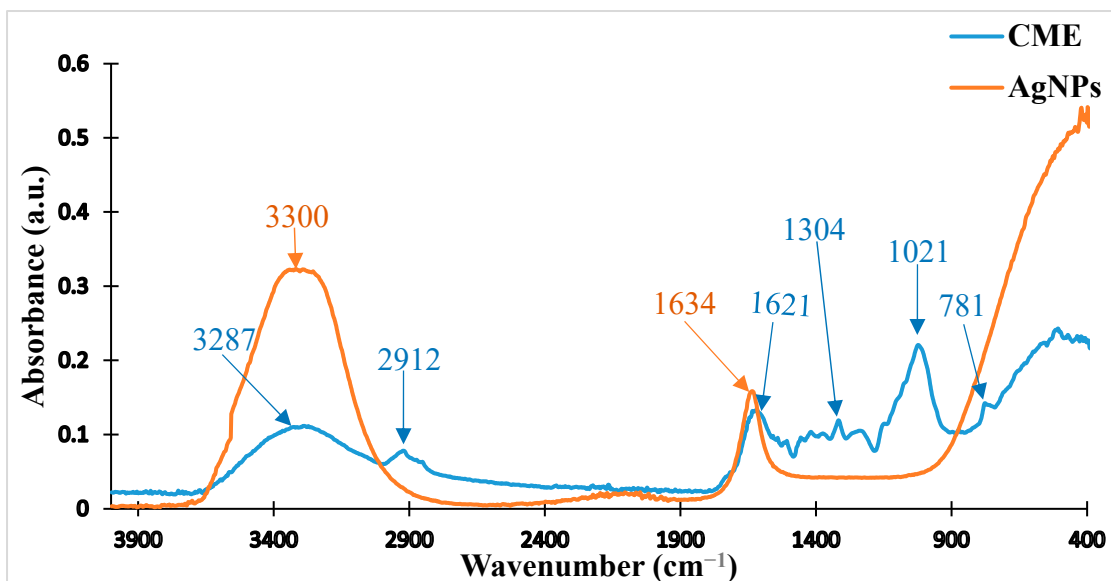


Figure 3. FTIR spectra of extract (CME) and nanoparticles (AgNPs) prepared from *C. macrostachyus* stem bark. AgNPs = silver nanoparticles; CME = *Croton macrostachyus* extract.

As evidenced by the characteristic peak revealed at 1634 cm^{-1} , the presence of proteins prevented the agglomeration of as-prepared nanoparticles. Indeed, it has been reported that capping proteins prevent agglomeration in the medium and are responsible for the fabrication of highly stable AgNPs [48]. As already reported by other authors [45,46], the absence of the peak that is characteristic of Ag-O groups indicates that silver is present in metallic form in the fabricated nanoparticles [49,50]. These results demonstrate that *C. macrostachyus* extract contains secondary metabolites, such as phenolics, flavonoids, alkaloids, and terpenoids [51], which might have been incorporated into the prepared nanoparticles.

2.3. Characterization of the As-Prepared Activated Carbon and Nanocomposites

2.3.1. FTIR of the Activated Carbon

Figure 4 shows the IR spectra of the activated carbon (orange color) and *C. macrostachyus* dried powder (blue color). It appears that both spectra differ in number and type of peaks. The very broad band observed around $3200\text{--}2500\text{ cm}^{-1}$ is attributed to the O-H elongation vibration association and may be characteristic of carbonyl and phenolic hydroxyl groups. The peak observed at 1574 cm^{-1} is characteristic of the C=C alkene groups of benzene. The frail peak that appears at 1156 cm^{-1} might be attributed to the P-O elongation from the phosphoric acid used in the activation. Another weak signal peak that appears at 1071 cm^{-1} corresponds to the in-plane deformation of the C-O groups of aromatic compounds and acetyl and carboxylic acid functions. The peaks that appear at 988 and 876 cm^{-1} indicate the presence of meta- and di-substituted benzene groups. Moreover, the presence of a haloalkane is indicated by the signal observed at 488 cm^{-1} . Notably, the peaks that were observed in the plant dried powder at 3287 and 2921 cm^{-1} disappeared after carbonization. In addition, the peak position was shifted to lower regions when *C. macrostachyus* dried powder was treated with phosphoric acid (H_3PO_4). The observed structural modifications have been attributed to the presence of organophosphorus compounds, which might overlay the outside plane deformation vibrations of C-H in the aromatic moieties [52].

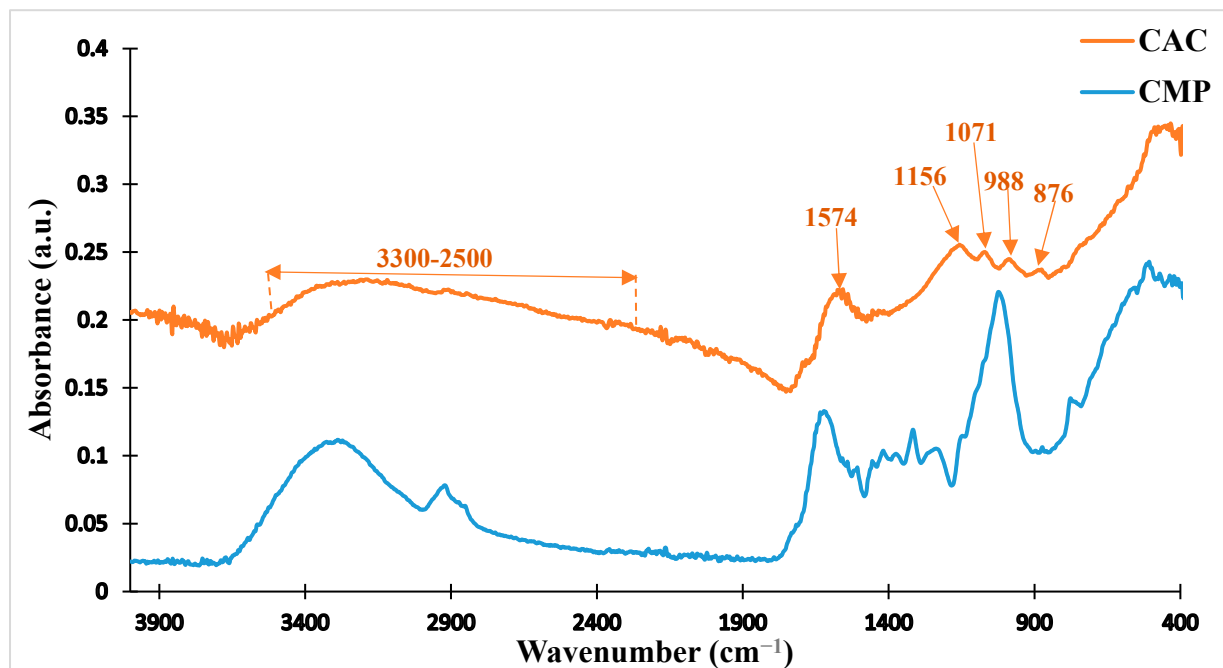


Figure 4. FTIR spectra of *C. macrostachyus* dried powder (CMP) and activated carbon (CAC). CAC = activated carbon; CMP = *Croton macrostachyus* dried powder.

2.3.2. FTIR of the Doped-Activated Carbon (Nanocomposite)

Figure 5 reveals the spectrum of the fabricated nanocomposite (orange color) compared to that obtained from the activated carbon (blue color). It can be seen that both spectra have almost the same pattern, indicating that the obtained nanocomposite is not a hybrid material and is structurally identical to the nanoparticle. A number of research groups have obtained the same results while working on the green synthesis of nanofillers and their nanocomposites [53,54].

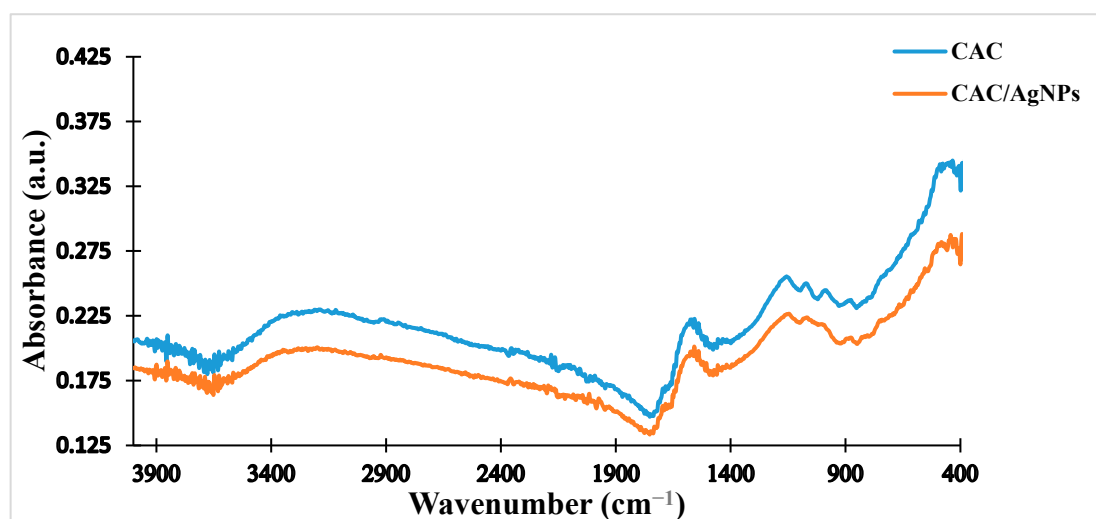


Figure 5. FTIR spectra of the activated carbon (CAC) and nanocomposite (CAC/AgNPs). CAC = activated carbon; CAC/AgNPs = nanocomposites.

2.3.3. Iodine Number and Methylene Blue Index

The identification of the iodine number and methylene blue index tests allowed for the characterization of microporosity (iodine), mesoporosity, and macroporosity (methylene blue) of the activated carbon and nanocomposite. Figure 6 shows the values of the iodine

number and methylene blue indices of the activated carbon and nanocomposite. The results demonstrate that the iodine number of the activated carbon (1026.69 mg/g) is higher than that of the nanocomposite (975.29 mg/g). These values corroborate those obtained by Islam et al. [55] (iodine number: 1000–1200 mg/g) and Raut et al. [56] (iodine number: 1140.69 mg/g) in their work on the fabrication and characterization of activated carbon from Jute Stick and sugarcane bagasse/rice husks, respectively [55,56]. Furthermore, the values of the methylene blue indices were almost identical for the activated carbon (89.862 mg/g) and nanocomposite (89.854 mg/g).

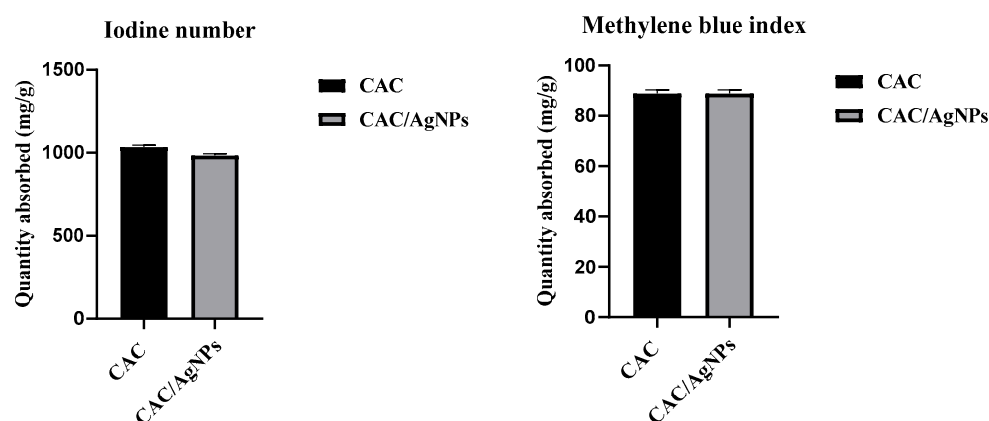


Figure 6. Quantitative analysis of iodine number and methylene blue indices of the activated carbon and nanocomposite. CAC = activated carbon; CAC/AgNPs = silver-doped nanomaterial. Data are presented as the mean \pm standard deviation. The histograms assigned to the stars are significantly different ($p < 0.0001$, Paired t -test).

As a partial conclusion, aqueous extracts, silver nanoparticles, activated carbon (percent in nanocomposite: 38.46%), and derived nanocomposite were successfully prepared from the stem bark of *Croton macrostachyus*. UV-visible spectra confirmed the synthesis of the nanoparticles. FTIR analysis revealed the presence of chemical functional groups that are characteristic of nanomaterials [57]. Notably, the effects of temperature and the activating agent (i.e., phosphoric acid) during the carbonization process (depolymerization and dehydration) were clearly demonstrated by differences in the spectra of the *Croton macrostachyus* extracts and activated carbon [58]. In addition, there were no significant changes in the spectra obtained for CAC and CAC/AgNPs, confirming the fabrication of the nanocomposite through van der Waals interactions [59]. Furthermore, the percentage of iodine number decreased by 5%, whereas the methylene blue index showed a percent reduction of 0.008%, inferring that, in lieu of macropores, the activated carbon's micropores constituted the main fixation site for the nanoparticles, leading to a decrease in their adsorption surface [49,60].

2.4. Antibacterial and Cytotoxic Activity Minimum Inhibitory Concentration

Table 1 summarizes the MIC values (range: 62.5 $\mu\text{g/mL}$ to $>1000 \mu\text{g/mL}$) of *C. macrostachyus* extract, the as-prepared activated carbon, nanoparticles, and nanocomposites. The median cytotoxic concentrations (CC_{50} s) of these entities for Vero cells are also presented in Table 1. The silver nanoparticles were the most active (MIC range: 62.5 to 125 $\mu\text{g/mL}$), followed by the nanocomposites (MIC range: 125 to 500 $\mu\text{g/mL}$). Although the nanocomposites were less active than the nanoparticles, their activity was superior when compared to that of the activated carbon (MIC $> 1000 \mu\text{g/mL}$). In fact, the antibacterial activity of the activated carbon (MIC $> 1000 \mu\text{g/mL}$) was potentiated by the incorporated nanoparticles. To our knowledge, no report has previously described the involvement of silver nanoparticles in potentiating the antibacterial activity of activated carbon obtained from the aqueous extract of *C. macrostachyus* stem bark. On the other hand, metal nanoparticles

are generally thought to be toxic because of the metal used during their fabrication as a result of their large specific surface area, high surface energy and magnetic interaction, as well as the easiness with which they agglomerate into micron- or millimeter-sized floccules [61]. Therefore, we attempted to overcome or minimize the toxicity caused by nanoparticles while maintaining their antibacterial activity by preparing nanocomposite counterparts using activated carbon. Furthermore, the most sensitive strain was found to be *Escherichia coli*, with MIC values of 62.5 and 125 µg/mL for AgNPs and CAC-AgNPs, respectively. These results are in agreement with those reported by Saiganesh et al. [62] demonstrating the anti-*Escherichia coli* effect of rare-earth ion lanthanum (La³⁺)-doped Nickel Oxide (NiO) nanoparticles obtained through green synthesis using *Sesbania grandiflora* leaf extract. Other reports have also pointed out inhibition of the growth of *Escherichia coli* by nanomaterials obtained from green synthesis using a natural polysaccharide pectin [63] and *Pimpinella anisum* seed extract [64].

Table 1. Minimum inhibitory (MIC) and median cytotoxic concentrations (CC₅₀).

	MICs (µg/mL)					CC ₅₀ s (µg/mL)	Selectivity Indices (SI)
	<i>E. coli</i>	<i>S. flexneri</i>	<i>S. sonnei</i>	<i>S. enteridis</i>	<i>S. aureus</i>		
CME	>1000	>1000	>1000	>1000	>1000	>1000	
CAC	>1000	>1000	>1000	>1000	>1000	396.5 ± 3.11	ND
AgNPs	62.5	125	125	125	125	164.75 ± 12.51	~2.64
CAC/AgNP	125	500	500	500	250	213.6 ± 1.41	~1.70
Ciprofloxacin	0.078	0.078	0.078	0.156	0.039	-	
Podophyllotoxin						0.4 ± 0.1	

AgNPs = silver nanoparticles; CAC = activated carbon; CAC/AgNP = doped activated carbon; CME = aqueous extract of *C. macrostachyus*; ND = not determined.

2.5. Effect of the As-Prepared Nanomaterials on the Mortality Kinetics of *S. aureus* and *E. coli*

The growth of *E. coli* and *S. aureus* was monitored for 24 h in the presence of nanoparticles (AgNPs) and nanocomposites (CAC/AgNPs) at a series of MIC value-based concentrations: MIC/4, MIC/2, MIC, 2MIC and 4MIC. As a result, both nanomaterials inhibited the growth of *E. coli* and *S. aureus* at MIC, 2MIC and 4MIC (Figures 7 and 8). Referring to Figure 7A,B, treatment with AgNPs decreased the bacterial population after 2 to 4 h of incubation time, followed by a stationary state of bacterial growth from 4 to 10 h of incubation time. In Figure 8A,B, the same trend was observed for treatment using various concentrations of the nanocomposites (CAC/AgNPs). In fact, after 4 h incubation time, there was bacterial growth, which was followed by a 6 h period (from 4 to 10 h incubation time) of no growth. From 10 h onwards, both *E. coli* and *S. aureus* resumed an exponential growth up to 24 h of incubation time upon treatment with both nanomaterials. The ephemeral bacterial growth inhibition (after 4h incubation time) caused by AgNPs and CAC/AgNPs led us to the conclusion that both nanomaterials induced a bacteriostatic effect as the bacterial growth resumed after 10 h of incubation and beyond. Notably, growth inhibition was concentration dependent, with higher MIC values (2MIC and 4MIC) resulting in greater activity, as evidenced by the trend in curves presented in Figures 7 and 8. However, ciprofloxacin, which was used as positive control did not show the same trend as this compound inhibited the bacterial growth in a continuous manner, whereas the untreated control group displayed exponential growth of bacteria from 0 to 24 h (Figures 7 and 8).

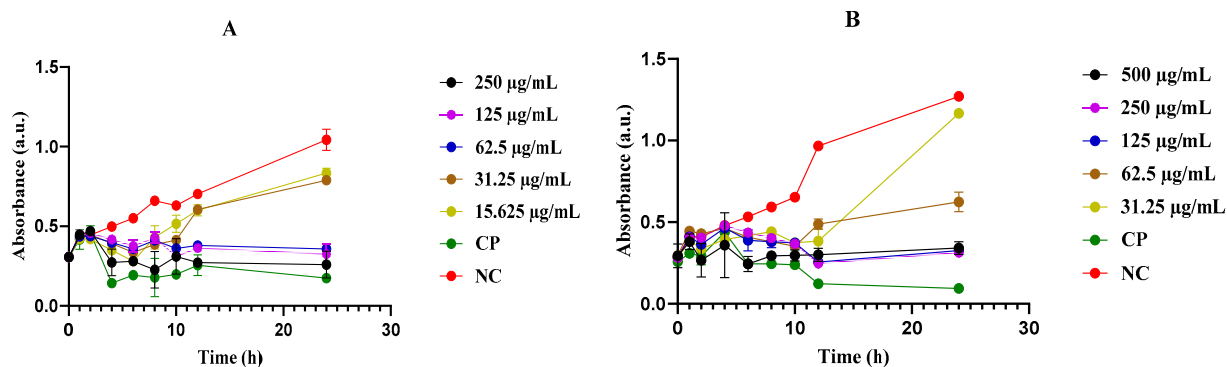


Figure 7. Growth inhibition kinetics of nanoparticles (AgNPs) against bacterial strains: (A) growth curve of *E. coli* and (B) growth curve of *S. aureus*. CP = ciprofloxacin, NC = negative control. Absorbance (a.u.) is at 630 nm. Data are presented as the mean \pm standard deviation. Significant differences are compared to the negative control ($p < 0.05$, Dunnett test).

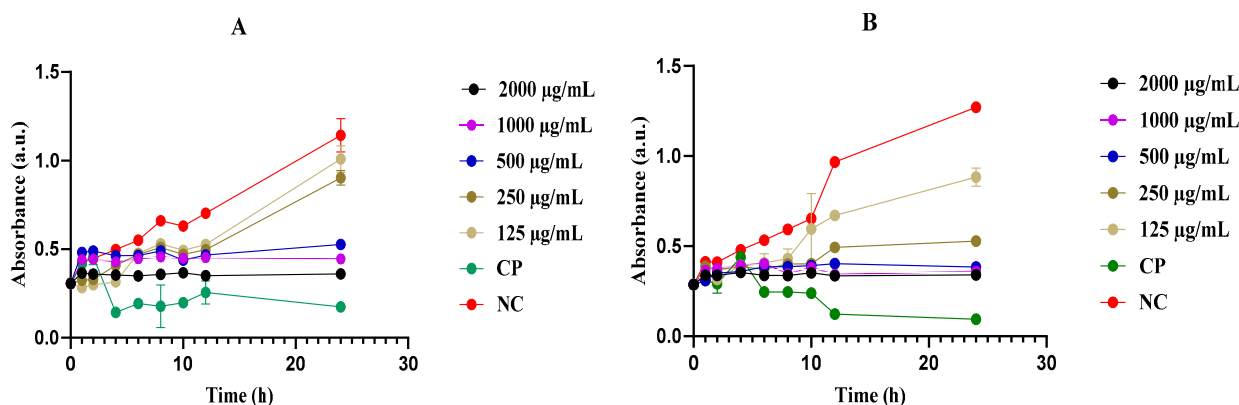


Figure 8. Growth inhibition kinetics of nanocomposites (CAC/AgNPs) against bacterial strains: (A) growth curve of *E. coli* and (B) growth curve of *S. aureus*. CP = ciprofloxacin, NC = negative control. Absorbance (a.u.) is at 630 nm. Data are presented as the mean \pm standard deviation. Significant differences are compared to the negative control ($p < 0.05$, Dunnett test).

2.6. Effect of Nanomaterials on the Membrane Integrity of *Escherichia coli* and *Staphylococcus aureus*

To evaluate the effect of the as-prepared nanomaterials on bacterial membrane integrity, cells were treated with MIC value-based concentrations (MIC/2, 2MIC and MIC) and incubated at incubation times varying from 0 to 8 h (0, 0.5, 1, 2, 4, 6 and 8 h). Next, the absorbance was measured at 260 nm (wavelength at which nucleic acid absorbs ultraviolet light) after 8 h of incubation time. Irrespective of the concentration tested, there was significant leakage of nucleic acids following bacterial treatment with AgNPs (Figure 9A,C) and CAC/AgNPs (Figure 9B,D). This observation suggests that the antibacterial mechanism of action of the as-prepared nanomaterials may be cell membrane disruption. Notably, due to their nanoscale size, nanomaterials anchor onto and easily penetrate and pass through the cell wall and interact with cell organelles [65,66]. Once in the bacteria, the nanomaterials interact with proteins, lipids, DNA lysosomes, ribosomes, and enzymes to inhibit normal cell function (oxidative stress, heterogeneous alterations, enzyme inhibition, changes in gene expression, among others) [28,67,68]. Although detailed antibacterial mechanisms of nanomaterials have not been fully elucidated, other reports point out the (i) induction of oxidative stress, (ii) release of the metal and metal oxide ions, (iii) and non-oxidative mechanisms [28,69].

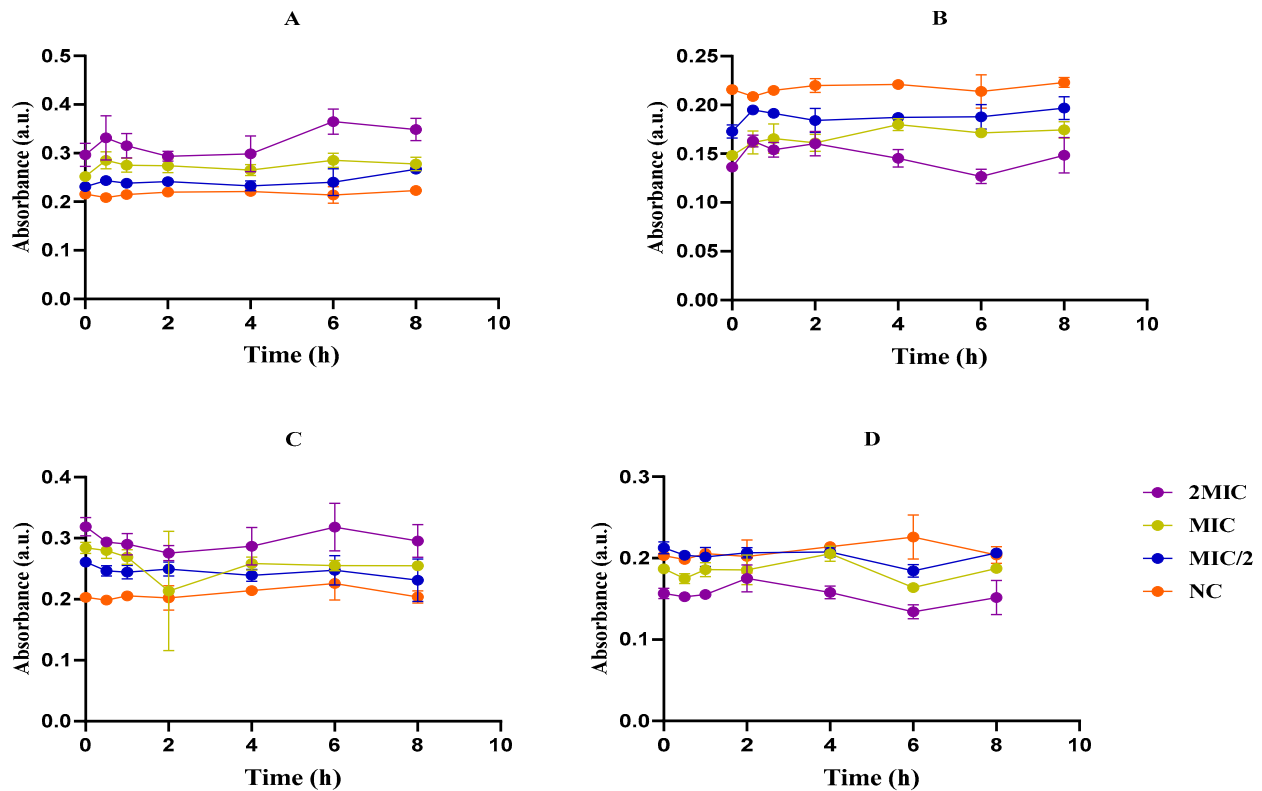


Figure 9. Effect of nanocomposites (CAC/AgNPs) and nanoparticles (AgNPs) on nucleic acid release from bacteria: (A) AgNPs on *S. aureus*, (B) CAC/AgNPs on *S. aureus*, (C) AgNPs on *E. coli*, and (D) CAC/AgNPs on *E. coli*. AgNPs = silver nanoparticles; CAC/AgNPs = nanocomposites; EC = *Escherichia coli*; MIC = minimum inhibitory concentration; NC = negative control; SA = *Staphylococcus aureus*. Data are presented as the mean \pm standard deviation. No significant differences were observed when compared with the negative control at $p < 0.05$, Dunnett test.

2.7. Catalase Inhibition Assay of the Nanomaterials

To evaluate the activity of catalase in *E. coli* and *S. aureus*, cells were treated with AgNPs and CAC/AgNPs along with hydrogen peroxide and PBS (phosphate buffer saline) for 30 min [70]. After reading the optical densities of the supernatant (obtained via centrifugation of the incubated preparation), the percentage of remaining H_2O_2 was calculated. For *E. coli*, the percentages of H_2O_2 remaining in the bacterial cultures after treatment varied from 2.45 to 6.02%, whereas, for *S. aureus*, these values ranged from 17.26 to 24.20% (Figure 10). Notably, the activity of the nanocomposites against catalase produced by both bacteria was superior to that of the nanoparticles. Widely distributed in aerobic and some anaerobic bacteria, catalase is an enzyme that is crucial in bacterial defense against oxidative stress [71,72]. Thus, it is not unreasonable to speculate that the as-prepared nanomaterials might have exerted antibacterial action by inhibiting the activity of catalase in *E. coli* and *S. aureus*.

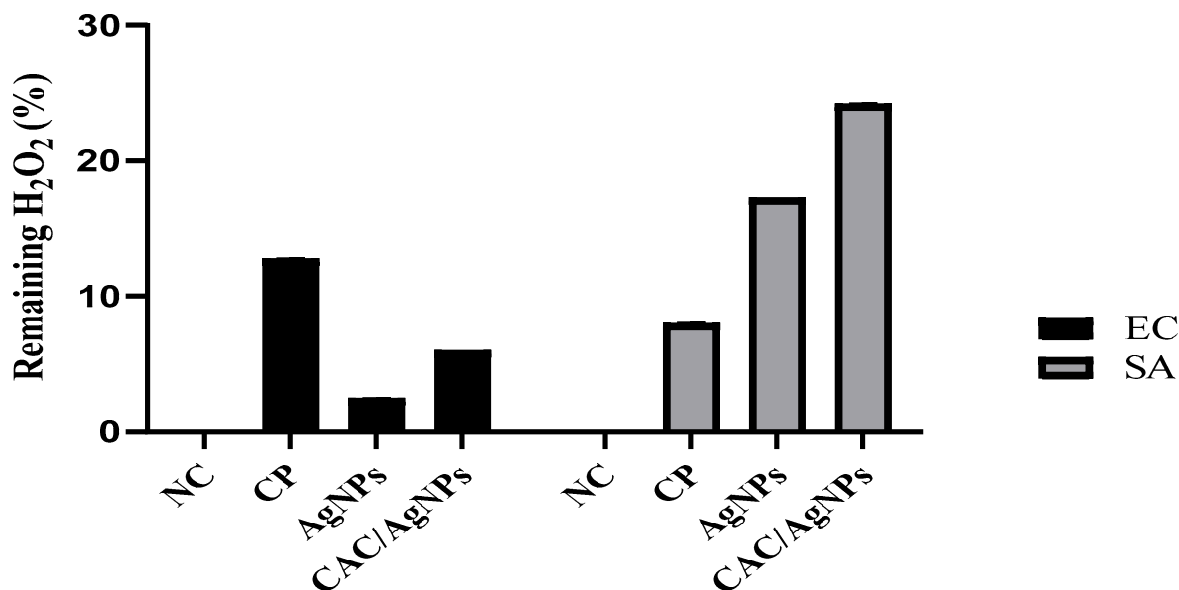


Figure 10. Effect of silver nanoparticles and nanocomposites on the catalase activity of *Escherichia coli* and *Staphylococcus aureus*. AgNP = nanoparticles; CAC/AgNP = nanocomposite; CP = ciprofloxacin; EC = *Escherichia coli*; CN = negative control; SA = *Staphylococcus aureus*. Data are presented as the mean \pm standard deviation. Significant differences are compared with negative control ($p < 0.05$, Dunnett test).

3. Material and Methods

3.1. Plant Collection and Identification

The plant material consisted of bark from the trunk of *Croton macrostachyus* that was collected in Baneghang (Penka-Michel, West Region, Cameroon) in March 2021. The identity of the plant was confirmed by Mr. Nana Victor (botanist) at the National Herbarium of Cameroon (Yaounde, Cameroon), where a voucher specimen was deposited under number 32264HNC.

3.2. Plant Extraction

The collected plant material was shade dried, then ground to fine powder using a grinder. Next, 10 g of bark powder was added to 500 mL of distilled water in an Erlenmeyer flask and boiled on a hot plate for 10 min. The resulting solution was allowed to cool to room temperature, then filtered through Wattman paper N°1. The filtrate was dried under ventilation for 4 days, and the extract was collected and kept at 4 °C for future use.

3.3. Preparation of Activated Carbon from *Croton macrostachyus*

The stem bark of *Croton macrostachyus* was washed with distilled water, cut into small pieces, and dried at room temperature (25 °C) in the dark. Next, the dried samples were ground and sieved to obtain finer particles. Prior to the fabrication of the activated carbon, an optimization study was carried out by varying three parameters (temperature, time and impregnation ratio) to obtain optimal reaction conditions. Firstly, preparation of the activated carbon was performed at different temperatures (300, 400 and 500 °C), after which the iodine number and methylene blue index were measured. At 400 °C, the highest values of iodine number and methylene blue index were obtained, and this temperature was considered as the optimal temperature for the fabrication of the activated carbon. Secondly, the time of the reaction was varied (1 h, 1 h 30 min and 2 h) to select the optimal time of reaction at 400 °C. The results showed that 1 h 30 min was the optimum time at which the activated carbon displays the highest iodine number and methylene blue index. Thirdly, the temperature and time of reaction were maintained at 400 °C and 1 h 30 min, respectively, while varying the impregnation ratio (1:1, 1:2 and 2:1) (dry plant

material: H_3PO_4). The 1:1 ratio was found to be the optimal impregnation ratio. After optimization studies, which allowed determination of the best carbonization conditions (temperature, time, and impregnation ratio), ten grams (10 g) of the fine powder (CMP) was impregnated with H_3PO_4 solution (1:1). The reaction mixture was left at room temperature for 1 h to allow for complete absorption into the *C. macrostachyus* stem bark. Afterward, the impregnated *C. macrostachyus* stem bark was dried at 110 °C for 24 h in an oven. The dried samples were kept temporarily in a desiccator, then carbonized at 400 °C for 1 h 30 min using a Carbolite Furnace to obtain the activated carbon (CAC). The obtained CAC was then washed to remove all impurities and dried at 110 °C for 12 h in an oven (Bluepard Instruments Co., Ltd., Shanghai, China).

3.4. Biological Synthesis and Characterization of Silver Nanoparticles Using *Croton macrostachyus*

3.4.1. Preparation of Silver Nanoparticles

For the synthesis of nanoparticles (AgNPs), 10 g of fine bark powder was added to 500 mL of distilled water in an Erlenmeyer flask and boiled on a hot plate for 10 min. The resulting solution was allowed to cool to room temperature and then filtered using Wattman paper number 1. One hundred milliliters (100 mL) of the obtained aqueous extract was added to 100 mL of 5 mM aqueous silver nitrate (AgNO_3) solution. Next, the mixture was stirred for 1 min using a magnetic stirrer (Horse shoe IKA magnetic agitator, Gemini Sustainable Lab Equipment, Apeldoorn, Netherlands) in the absence of light to avoid any photochemical reactions of silver nitrate and stored in a dark chamber for 24 h. The generation of the nanoparticles was evidenced by the color change from pale yellow to dark brown. The absorbance of the resulting solution was read using a visible ultraviolet spectrophotometer.

3.4.2. Characterization of AgNPs

The as-prepared silver nanoparticles were characterized using analytical techniques such as UV–visible (UV–Vis) spectrophotometry and Fourier transform infrared (FTIR).

UV–Vis Spectrophotometry Analysis

The UV–visible analysis of the extracts and prepared nanoparticles (AgNPs) was carried out using a Shimadzu UV–visible spectrophotometer (UV-1800, Cole-Parmer Instrument Company Llc, Yusaki LLC, Tondabayashi City, Osaka Prefecture, Japan) in the wavelength range of 350–900 nm to obtain UV–visible spectra of the sample.

Fourier Transform Infrared Spectroscopy Analysis of AgNPs

FTIR analysis of the aqueous extract and AgNPs was performed in the absorbance range of 400 to 4000 cm^{-1} using a Universal ATR (crystal: platinum, diamond; bounces: 1; solvent: ethanol). In brief, the prepared extract or nanoparticles (AgNPs) were mixed with potassium bromide (KBr) and subsequently pressed into pellets. The pellets thus formed by compression were placed in the sample holder of the apparatus for analysis. The results of the transmittance as a function of wavelength were given by the screen. Afterwards, the obtained spectrograms were analyzed to identify the functional groups located on the surface of the extract and nanoparticles.

3.5. Preparation and Characterization of Nanocomposites Prepared from *Croton macrostachyus*

3.5.1. Preparation of the Nanocomposites

To obtain the nanocomposites (CAC/AgNPs), the silver nanoparticles (AgNPs) were loaded onto the activated carbon (CAC) by means of simple agitation as previously reported by Odogu et al. [49]. Briefly, 5.0 g of CAC was added to 200 mL of AgNP solution, then the resulting solution was vigorously mixed by continuous stirring for 1 h at 150 rpm using a Horse shoe IKA agitator. The nanocomposites were obtained by drying the AgNP-loaded activated carbon powder at 110 °C in an oven (Bluepard Instruments Co., Ltd., Shanghai, China).

3.5.2. Characterization of the Adsorbents Activated Carbon and Nanocomposites

The as-prepared activated carbon (CAC) and nanocomposites (CAC/AgNPs) were characterized by determining methylene blue and iodine numbers. FTIR measurements were carried out to detect changes in the composition of biomolecules and their functional groups. FTIR analysis was performed in the absorbance range of 400 to 4000 cm^{-1} using a Universal ATR (crystal: platinum, diamond; bounces: 1; solvent: ethanol).

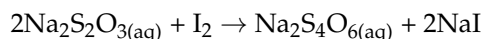
3.5.3. Determination of the Methylene Blue Index and Iodine Number

Defined as the number of milligrams of iodine or methylene blue adsorbed by 1 g of activated carbon, the iodine number and methylene blue index, respectively, provide information on the microporosity (up to 2 nm) and mesoporosity of activated carbon. The porosity of activated carbon is critical for assessing the degree of adsorption of metal loaded-activated carbon for a given molecular size.

Determination of the Iodine Number Using Batch Mode Adsorption

To determine the iodine number, 100 mg of CAC and CAC/AgNPs were separately introduced into 30 mL of iodine solution in 100 mL Erlenmeyer flasks. Then, the mixtures were sealed and stirred for 3 h at room temperature. After stirring, each mixture was filtered through a Wattman filter paper, and the filtrate obtained was collected in a dry flask.

Next, 10 mL of each solution was titrated with sodium thiosulfate using starch as an indicator until the solution became transparent. The equation for this reaction is as follows:



The amount of iodine adsorbed is given by the following formula (Nasehir et al., 2010) [73]:

$$Q = \frac{(\text{Co} - \text{Ce}) \times V}{m_{\text{CAP}}}$$

where Co is the initial concentration of methylene blue; Ce is the equilibrium concentration of methylene blue; m represents the mass (g) of sample (CAC or CAC/AgNPs); and V is the volume of methylene blue solution.

Determination of the Methylene Blue Index Using Batch Mode Adsorption

To determine the methylene blue index, 100 mg of CAC and CAC/AgNPs was separately introduced into 30 mL of methylene blue solution in 100 mL Erlenmeyer flasks. Then, the mixtures were sealed and stirred for 3 h at room temperature. After stirring, each mixture was filtered using a Wattman filter paper number 1 and the filtrate obtained was collected in a dry flask. Next, the absorbance was read at 660 nm against the blank using a spectrophotometer (Spectrumlab S23A, Wincom Company Ltd., Changsha Hunan, China). The amount of methylene blue adsorbed was calculated using the following formula [73]:

$$Q = \frac{(\text{Co} - \text{Ce}) \times V}{m_{\text{CAP}}}$$

where Co is the initial concentration of methylene blue; Ce is the equilibrium concentration of the methylene blue; m represents the mass (g) of sample (CAC or CAC/AgNPs); and V is the volume of methylene blue solution.

3.6. Antibacterial Activity

The antibacterial activity of the *C. macrostachyus* extract and synthesized nanomaterials was assessed on five bacterial strains according to the guidelines set by the Clinical Laboratory Standards Institute [74] using 96-well microtitre plates. The bacterial strains used in this study are summarized in Table 2. *Shigella flexneri* and *Shigella sonnei* were generously obtained from the Biodefense and Emerging Infections Research Resources Repository (BEI Resources, Rockville, MD 20,852), whereas *Escherichia coli* and *Staphylococ-*

cus aureus were obtained commercially from the American Type Culture Collection (ATCC, Manassas, VA, USA). *Salmonella enteridis* was generously obtained from the Centre Pasteur of Cameroon (CPC).

Table 2. List of bacterial strains used for anti-bacterial activity.

Bacterial Strains	Acronym	Reference Number	Supplier
<i>Escherichia coli</i>	<i>E. coli</i>	ATCC 25922	ATCC
<i>Salmonella enteridis</i>	<i>S. enteridis</i>	Isolat	CPC
<i>Shigella flexneri</i>	<i>S. flexneri</i>	NR 518	BEI resources
<i>Shigella sonnei</i>	<i>S. sonnei</i>	NR 519	BEI resources
<i>Staphylococcus aureus</i>	<i>S. aureus</i>	ATCC 43300	ATCC

ATCC = American Type Culture Collection; BEI Resources = Biodefense and Emerging Infections Research Resources Repository; CPC = Centre Pasteur of Cameroon.

Briefly, 96 μ L of Mueller Hinton Broth (MHB) culture medium was introduced into each well of a 96-well plate followed by subsequent addition of 4 μ L of stock solution of each prepared sample (extract of AgNPs) at 100 mg/mL. Next, 100 μ L of 1×10^6 mL of inoculum was added to each well except those for the sterility control. The positive control consisted of the inoculum and ciprofloxacin (10 μ g/mL). The negative control comprised culture medium and inoculum, whereas the sterility control consisted of culture medium only. The plates were covered and incubated at 37 $^{\circ}$ C for 24 h. At the end of the incubation period, 20 μ L of freshly prepared resazurin solution (0.15 mg/mL) was added to each well, and the plates were once again incubated under the same conditions for 30 min. The wells in which there was no visible bacterial growth corresponded to those containing active substances. Extracts and nanoparticles that inhibited the growth of bacteria at 1000 μ g/mL concentration were selected for the determination of minimum inhibitory concentrations (MICs).

3.7. Determination of Minimum Inhibitory Concentrations

Minimum inhibitory concentrations (MICs) of the doped activated carbon and nanoparticles from *C. macrostachyus* were determined by the broth microdilution method, using the microdilution assay as described above. The assays were performed in duplicate in sterile 96-well microplates. In brief, 196 μ L of MHB culture medium was introduced into the wells of column A, while 100 μ L was added to the remaining wells of the microplate. Subsequently, 4 μ L of a sterile solution of the extract, nanoparticles (AgNPs), or nanocomposites (CAC/AgNPs) (100 mg/mL) was added into the wells of column A. This addition was followed by the preparation of eight serial 2-fold dilutions in columns A to H. Next, 100 μ L of bacterial load *viz.* 1×10^6 UFC/mL was distributed to the remaining wells, including negative control wells. The concentrations of extract or nanoparticles and ciprofloxacin in the wells of a row ranged from 1000 μ g/mL to 7.8125 μ g/mL and from 5 μ g/mL to 0.15625 μ g/mL, respectively. The sterility control contained the culture medium only, whilst the positive control was made up of culture medium, inoculum, and ciprofloxacin (stock solution at 1 mg/mL). The microplates were coated and then incubated at 37 $^{\circ}$ C for 24 h. Next, 20 μ L of freshly prepared resazurin solution (0.15 mg/mL) was added to all wells, and the plates were incubated again at 37 $^{\circ}$ C for 30 min. The lowest concentration at which no color change (from blue to pink) is observed corresponds to the absence of bacterial growth and is considered the MIC value.

3.8. Cytotoxicity Assays

The cytotoxicity of the most active nanomaterials was assessed on human mammalian cells (Vero cell line ATCC CRL 1586) using the resazurin colorimetric method as described by Bowling et al. [75]. The Vero cell line (ATCC CRL 1586) was cultured in complete medium containing 13.5 g/L DMEM (Gibco, Waltham, MA, USA), 0.5% MEM (Gibco, Waltham, MA, USA), 10% fetal bovine serum (Gibco, Waltham, MA, USA), 0.21% bicarbonate (Sigma-

Aldrich, New Delhi, India), and 10 mL (1%) of penicillin/streptomycin antibiotics. Briefly, 100 μ L of cell suspension was introduced into 96-well (CosStar, Washington, DC, United States of America) microplates (10^4 cells per well) and incubated overnight (18 h) to allow cell adhesion. Subsequently, the culture medium was replenished with 90 μ L of fresh complete culture medium, and then 10 μ L of serially diluted extract or nanoparticles was added in triplicate to the corresponding wells. Podophyllotoxin at 50 μ M was used as a positive control, and wells involving untreated cells were included as a 100% growth control. Next, the plates were incubated in a humidified atmosphere with 5% CO₂ at 37 °C for 48 h. Afterwards, 10 μ L of resazurin stock solution (0.15 mg/mL in phosphate buffer saline, PBS) was added to each well and incubated for an additional 4 h. Fluorescence was then read using a multi-well plate reader (TECAN-Infinite M200, Tecan Austria GmbH, Grödig Flachgau, Austria) at excitation and emission wavelengths of 530 and 590 nm, respectively. From the optical densities (OD) obtained, percentages of cell viability were calculated according to the following formula:

$$\text{Percentages of cell viability(\%)} = \frac{\text{OD test}}{\text{OD negative control}} \times 100$$

Percentages of cell viability were used to determine the median cytotoxic concentrations (CC₅₀) using nonlinear regression curves using GraphPad Prism 5.0 (San Diego, CA, USA) software.

3.9. Potential Mechanistic Studies of the Most Potent Nanomaterials

To understand the mechanism of antibacterial action, growth kinetics, release of nucleic acids by bacteria and inhibition of catalase upon treatment with the most promising nanoparticles (AgNPs) and nanocomposites (CAC/AgNPs) were investigated.

3.9.1. Bacterial Growth Kinetics Resulting from Various Concentrations of Nanomaterials

To study the bacterial growth curve, cultures containing *E. coli* and *S. aureus* strains were incubated with the most active antibacterial nanoparticles (AgNPs) and nanocomposites (CAC/AgNPs) as per the protocol reported by Nguimatsia et al. [76] with minor modifications. In short, 20 μ L of AgNPs and 8 μ L of CAC/AgNPs were added to 180 μ L and 192 μ L of Mueller Hinton Broth, respectively, in the first twelve wells of column A (A). In the remaining wells of the microplate, 100 μ L of Mueller Hinton Broth was introduced. Next, 2-fold serial dilutions were prepared in columns A to H to achieve concentrations ranging from 250 to 15.625 μ g/mL and from 2000 to 125 μ g/mL for AgNPs and CAC/AgNPs, respectively. Afterwards, 100 μ L of 1×10^6 UFC/mL inoculum was introduced into each well except for the control groups (sterility, AgNPs, and CAC/AgNPs). Ciprofloxacin was used as a positive control. The microplate was coated and incubated at 37 °C for diverse incubation time periods (0, 1, 2, 4, 6, 8, 10, 12 and 24 h), and the optical densities were read at 630 nm using a microplate reader (Infinite M200 microplate reader TECAN, Männedorf, Switzerland) after each incubation time had elapsed. The values obtained were used to plot OD = f(t) graphs.

3.9.2. Nucleic Acid Leakage Assays

This test was performed according to the protocol described by Carson et al. [77]. The assays were performed in triplicate in 2 mL eppendorf tubes. Colonies obtained from 24 h cultures were washed twice with NaCl solution (0.9%) then resuspended in sterile peptone water (0.1%) and calibrated to 0.5 MacFarland standard. Subsequently, 250 μ L of inoculum (1.5×10^8 UFC/mL) was introduced into 250 μ L of peptone water containing the prepared extract at different concentrations (2CMI, CMI, and CMI/2), and the tubes were incubated at 37 °C for different times (0, 0.5, 1, 2, 4, 6 and 8 h). After each incubation period, the solution was centrifuged at 5000 rpm for 20 min. The supernatant was collected and transferred into wells of a microplate, and the absorbance was measured at 260 nm using a

TECAN infinite M200 plate reader. The obtained optical densities (OD) were plotted versus time using Excel software (version 2013, Washington, DC, USA).

3.9.3. Catalase Inhibition Assay

Catalase inhibition by the most active nanoparticles (AgNPs) or nanocomposites (CAC/AgNPs) was determined for *E. coli* ATCC 25922 and *S. aureus* ATCC 43300 according to a previously described protocol [63]. The assays were performed in triplicate in 2 mL eppendorf tubes. Various concentrations of samples (AgNPs and CAC/AgNPs) were introduced to test tubes containing 200 μ L of hydrogen peroxide (40 mM) and 200 μ L of phosphate buffer saline (PBS 10X; pH = 7.3–7.7) (Sigma-Aldrich, Darmstadt, Germany). Next, 100 μ L aliquots of bacterial suspension (1.5×10^8 CFU/mL) were added to these mixtures, and the samples were incubated at 37 °C for 30 min. Then, the test tubes were centrifuged at 1200 rpm for 10 min, and the supernatant was collected and transferred into wells of a microplate. Finally, the optical density of the microplate was read against the blank (phosphate buffer saline, PBS 10X, pH: 7.3–7.7) and the negative control (bacteria in PBS without inhibitor) at 232 nm using an Infinite M200 microplate reader (TECAN, Männedorf, Switzerland). Ciprofloxacin (at 0.078 and 0.039 μ g/mL for *E. coli* ATCC 25922 and *S. aureus* ATCC 43300, respectively) was used as a positive control. The percentage of remaining hydrogen peroxide was determined according to the following formula:

$$\% \text{ of remaining H}_2\text{O}_2 = \frac{(Ae - Ac)}{Ac} \times 100$$

where Ac is the negative control and Ae is the absorbance of H₂O₂ in the presence of the sample.

3.9.4. Statistical Analysis

Results were expressed as the mean \pm standard deviation. The statistical analysis and plots were performed using Graphpad Prism 8 and Excel software (version 2013, Washington, DC, USA). The means were analyzed using one-way ANOVA (analysis of variance) tests, followed by a multiple comparison (Dunnett test), and were considered significant for $p < 0.05$.

4. Limitations and Perspectives

The present preliminary report highlights the scientific validation of the use of plants (*Croton macrostachyus* stem bark) and products (nanomaterial) as starting points for the discovery of antimicrobial agents of natural origin. Moreover, the mechanistic basis of the antibacterial action demonstrated that the nanomaterials induced (i) bacteriostatic activity vis-à-vis *E. coli* and *S. aureus* and (ii) inhibition of catalase in these bacteria. Furthermore, a versatile characterization tool, FTIR, was employed to characterize the surface and chemical composition of the nanomaterials. In addition, the concentration and optical and structural properties of the nanoparticles were evaluated through UV-vis.

This novel contribution regarding the antibacterial mechanisms of action of silver nanocomposites from *C. macrostachyus*-based activated carbon may help us to better understand the bacterial inhibition by this biomaterial. However, major limitations of this study include assessment of the nanoparticle's parameters, including shape, crystal structure, and surface charge through characterization techniques, such as TEM, XRD, among others. Nevertheless, to unravel the complete characterization of the prepared nanomaterials, assessment of morphological features such as crystal structure and surface charge, etc. using XRD and TEM analyses should be considered as a perspective to this work. In addition, in vivo experiments as well as in depth antibacterial mechanistic studies are warranted to ensure the successful utilization of these antibacterial biomaterials.

5. Conclusions

To sum up, an eco-friendly method was developed to synthesize silver nanocomposites from corresponding nanoparticles and *C. macrostachyus*-based activated carbon. The nanomaterials were further characterized using UV–visible spectroscopy and FTIR analyses. The nanomaterials exhibited antibacterial activity against an array of bacterial strains, the most susceptible being *Escherichia coli* and *Staphylococcus aureus*. Although the activated carbon did not exhibit antibacterial action, their role in minimizing the cytotoxicity of the nanocomposite was paramount. Antibacterial mechanistic studies revealed that the as-prepared nanomaterials induced (i) bacteriostatic activity vis à vis *E. coli* and *S. aureus* and (ii) inhibition of catalase in these bacteria. This novel contribution regarding the antibacterial mechanisms of action of silver nanocomposites from *C. macrostachyus*-based activated carbon may help us to better understand the bacterial inhibition by this biomaterial. The results suggest that the prepared nanocomposite is a promising antibacterial candidate with low toxicity to Vero cells.

Author Contributions: Conceptualization, P.K.L., J.N.N. and F.F.B.; methodology, P.K.L., J.N.N., F.L.T.T., B.P.K., V.L.Y. and Z.Y.T.; software, F.L.T.T.; validation, P.K.L., J.N.N. and F.F.B.; formal analysis, F.L.T.T., Z.Y.T., V.L.Y., B.P.K. and V.N.; investigation, F.L.T.T., B.P.K. and V.N.; resources, P.K.L., J.N.N. and F.F.B.; data curation, F.L.T.T., B.P.K. and V.N.; writing—original draft preparation, F.L.T.T., B.P.K. and V.N.; writing—review and editing, F.L.T.T., B.P.K. and V.N.; visualization, P.K.L.; supervision, P.K.L., J.N.N. and F.F.B.; project administration, P.K.L., J.N.N., B.P.K. and F.F.B.; funding acquisition, P.K.L., J.N.N. and F.F.B. All authors have read and agreed to the published version of the manuscript.

Funding: This research received external funding from the Yaounde–Bielefeld Bilateral Graduate School for Natural Products with Anti-parasite and Antibacterial Activity (YaBiNaPA) (grant number 57316173) and Seeding Labs’ Instrumental Access.

Institutional Review Board Statement: Not applicable.

Informed Consent Statement: Not applicable.

Data Availability Statement: Data is available from the corresponding author upon reasonable request. The data are not publicly available due to the sensitive nature of the research supporting data.

Acknowledgments: Authors are thankful to the Cameroon National Herbarium (Yaounde, Cameroon) for their assistance with plant identification. The authors also acknowledge the “Centre Hospitalier Universitaire” of Yaounde–Cameroon and “Centre Pasteur” of Cameroon for providing the bacterial strains species. This work was supported by and also received material and equipment support from the Yaounde–Bielefeld Bilateral Graduate School for Natural Products with Anti-parasite and Antibacterial Activity (YaBiNaPA) and Seeding Labs’ Instrumental Access.

Conflicts of Interest: The authors declare no conflict of interest.

References

1. The World Health Organization (WHO). Shigella. The Fact Sheets. 2023. Available online: <https://www.who.int/teams/immunization-vaccines-and-biologicals/diseases/shigella> (accessed on 5 October 2023).
2. Cleveland Clinic (CC). Infectious Diseases. 2023. Available online: <https://my.clevelandclinic.org/health/diseases/17724-infectious-diseases> (accessed on 7 October 2023).
3. The World Health Organization (WHO). The Key Facts. Antibiotic Resistance. 2023. Available online: <https://www.who.int/news-room/fact-sheets/detail/antibiotic-resistance> (accessed on 6 October 2023).
4. Reygaert, W.C. An overview of the antimicrobial resistance mechanisms of bacteria. *AIMS Microbiol.* **2018**, *4*, 482–501. [[CrossRef](#)] [[PubMed](#)]
5. Neu, H.C.; Gootz, T.D. Basis of Antimicrobial Action; General Concepts; Medical Microbiology. Chapter 11: Antimicrobial Chemotherapy. In *Medical Microbiology*, 4th ed.; Baron, S., Ed.; University of Texas Medical Branch at Galveston: Galveston, TX, USA, 1996; pp. 1–17.
6. Jeśman, C.; Młodzik, A.; Cybulska, M. History of antibiotics and sulphonamides discoveries. *Pol. Merkur. Lek.* **2011**, *30*, 320–322. [[PubMed](#)]
7. Bhattacharjee, M.K. Antimetabolites: Antibiotics that inhibit nucleotide synthesis. Book Chapter. In *Chemistry of Antibiotics and Related Drugs*; Springer: Berlin/Heidelberg, Germany, 2016; pp. 109–123.

8. Estrada, A.; Wright, D.L.; Anderson, A.C. Antibacterial antifolates: From development through resistance to the next generation. *Cold Spring Harb. Perspect. Med.* **2016**, *6*, a028324. [[CrossRef](#)] [[PubMed](#)]
9. Fisher, J.F.; Mobashery, S. β -Lactams from the Ocean. *Mar Drugs* **2023**, *21*, 86. [[CrossRef](#)] [[PubMed](#)]
10. Smith, P.W.; Zuccotto, F.; Bates, R.H.; Martinez-Martinez, M.S.; Read, K.D.; Peet, C.; Epemolu, O. Pharmacokinetics of β -lactam antibiotics: Clues from the past to help discover long-acting oral drugs in the future. *ACS Infect. Dis.* **2018**, *4*, 1439–1447. [[CrossRef](#)]
11. Cambau, E.; Guillard, T. Antimicrobials that affect the synthesis and conformation of nucleic acids. *Rev. Sci. Tech.* **2012**, *31*, 77–87. [[CrossRef](#)]
12. Fernández-Villa, D.; Aguilar, M.R.; Rojo, L. Folic acid antagonists: Antimicrobial and immunomodulating mechanisms and applications. *Int. J. Mol. Sci.* **2019**, *20*, 4996. [[CrossRef](#)]
13. Kannan, K.; Mankin, A.S. Macrolide antibiotics in the ribosome exit tunnel: Species-specific binding and action. *Ann. N. Y. Acad. Sci.* **2011**, *1241*, 33–47. [[CrossRef](#)]
14. Aslam, B.; Wang, W.; Arshad, M.I.; Khurshid, M.; Muzammil, S.; Rasool, M.H.; Nisar, M.A.; Alvi, R.F.; Aslam, M.A.; Qamar, M.U.; et al. Antibiotic resistance: A rundown of a global crisis. *Infect. Drug Resist.* **2018**, *11*, 1645–1658. [[CrossRef](#)]
15. Ghosh, A.; Jayaraman, N.; Chatterji, D. Small-molecule inhibition of bacterial biofilm. *ACS Omega* **2020**, *5*, 3108–3115. [[CrossRef](#)]
16. World Health Organisation. WHO methods and data sources for global burden of disease estimates 2000–2011. In *Geneva: Department of Health Statistics and Information Systems*; WHO: Geneva, Switzerland, 2013. Available online: https://cdn.who.int/media/docs/default-source/gho-documents/global-health-estimates/gh2019_daly-methods.pdf (accessed on 5 October 2023).
17. Tang, S.; Zheng, J. Antibacterial activity of silver nanoparticles: Structural effects. *Adv. Healthc. Mater.* **2018**, *7*, 1701503. [[CrossRef](#)] [[PubMed](#)]
18. Ugboke, H.U.; Nwinyi, O.C.; Oranusi, S.U.; Fatoki, T.H.; Omonhinmin, C.A. Antimicrobial importance of medicinal plants in Nigeria. *Sci. World J.* **2020**, *2020*, 1–10. [[CrossRef](#)] [[PubMed](#)]
19. Abdallah, E.M.; Alhatlani, B.Y.; Menezes, R.d.P.; Martins, C.H.G. Back to nature: Medicinal plants as promising sources for antibacterial drugs in the post-antibiotic era. *Plants* **2023**, *12*, 3077. [[CrossRef](#)] [[PubMed](#)]
20. Mody, V.V.; Siwale, R.; Singh, A.; Mody, H.R. Introduction to metallic nanoparticles. *J. Pharm. Bioallied Sci.* **2010**, *2*, 282–289. [[CrossRef](#)] [[PubMed](#)]
21. Zomuansangi, R.; Singh, B.P.; Singh, G.; Puia, Z.; Singh, P.K.; Song, J.J.; Kharat, A.S.; Deka, P.; Yadav, M.K. Chapter 14—Role of nanoparticles in the treatment of human disease: A comprehensive review. In *Nanotechnology and Human Health. Current Research and Future Trends. Nanotechnology in Biomedicine*; Elsevier: Amsterdam, The Netherlands, 2023; pp. 381–404.
22. Makvandi, P.; Wang, C.y.; Zare, E.N.; Borzacchiello, A.; Niu, L.n.; Tay, F.R. Metal-based nanomaterials in biomedical applications: Antimicrobial activity and cytotoxicity aspects. *Adv. Funct. Mat.* **2020**, *30*, 1910021. [[CrossRef](#)]
23. Susanti, D.; Haris, M.S.; Taher, M.; Khotib, J. Natural products-based metallic nanoparticles as antimicrobial agents. *Front. Pharmacol.* **2022**, *13*, 895616. [[CrossRef](#)] [[PubMed](#)]
24. Dolai, J.; Mandal, K.; Jana, N.R. Nanoparticle size effects in biomedical applications. *ACS Appl. Nano Mater.* **2021**, *4*, 6471–6496. [[CrossRef](#)]
25. Chandraker, S.K.; Kumar, R. Biogenic biocompatible silver nanoparticles: A promising antibacterial agent. *Biotechnol. Genet. Eng. Rev.* **2022**, *2*, 1–35. [[CrossRef](#)]
26. Dakal, T.C.; Kumar, A.; Majumdar, R.S.; Yadav, V. Mechanistic basis of antimicrobial actions of silver nanoparticles. *Front. Microbiol.* **2016**, *7*, 1831. [[CrossRef](#)]
27. Franci, G.; Falanga, A.; Galdiero, S.; Palomba, L.; Rai, L.; Morelli, G.; Galdiero, M. Silver nanoparticles as potential antibacterial agents. *Molecules* **2015**, *20*, 8856–8874. [[CrossRef](#)]
28. Wang, L.; Hu, C.; Shao, L. The antimicrobial activity of nanoparticles: Present situation and prospects for the future. *Int. J. Nanomed.* **2017**, *12*, 1227–1249. [[CrossRef](#)] [[PubMed](#)]
29. Motelica, L.; Ficai, D.; Oprea, O.C.; Ficai, A.; Ene, V.L.; Vasile, B.S.; Andronesu, E.; Holban, A.M. Antibacterial biodegradable films based on alginate with silver nanoparticles and lemongrass essential oil-innovative packaging for cheese. *Nanomater* **2021**, *11*, 2377. [[CrossRef](#)] [[PubMed](#)]
30. Yu, L.; Tatsumi, D.; Kondo, T. Preparation of carbon nanoparticles from activated carbon by aqueous counter collision. *J. Wood Sci.* **2022**, *68*, 29. [[CrossRef](#)]
31. Marinescu, L.; Ficai, D.; Oprea, O.; Marin, A.; Ficai, A.; Andronesu, E.; Holban, A.-M. Optimized synthesis approaches of metal nanoparticles with antimicrobial applications. *J. Nanomater.* **2020**, *2020*, 6651207. [[CrossRef](#)]
32. Pongener, C.; Kibami, D.; Rao, K.S.; Goswamee, R.L.; Sinha, D. Adsorption studies of fluoride by activated carbon prepared from *Mucuna prurines* plant. *J. Water Chem. Technol.* **2017**, *39*, 108–115. [[CrossRef](#)]
33. Burchacka, E.; Pstrowska, K.; Bryk, M.; Maciejowski, F.; Kułażyński, M.; Chojnacka, K. The properties of activated carbons functionalized with an antibacterial agent and a new SufA protease inhibitor. *Materials* **2023**, *16*, 1263. [[CrossRef](#)] [[PubMed](#)]
34. Rivera-Utrilla, J.; Bautista-Toledo, I.; Ferro-Garca, M.A.; Moreno-Castilla, C. Activated carbon surface modifications by adsorption of bacteria and their effect on aqueous lead adsorption. *J. Chem. Technol. Biotechnol.* **2001**, *76*, 1209–1215. [[CrossRef](#)]
35. Balashanmugam, P.; Kalaichelvan, P.T. Biosynthesis characterization of silver nanoparticles using *Cassia roxburghii* DC. aqueous extract, and coated on cotton cloth for effective antibacterial activity. *Int. J. Nanomed.* **2015**, *10*, 87–97. [[CrossRef](#)]

36. Wibawa, P.J.; Nur, M.; Asy'ari, M.; Wijanarka, W.; Susanto, H.; Sutanto, H.; Nur, H. Green synthesized silver nanoparticles immobilized on activated carbon nanoparticles: Antibacterial activity enhancement study and its application on textiles fabrics. *Molecules* **2021**, *26*, 3790. [[CrossRef](#)]
37. Ameen, F.; Karimi-Maleh, H.; Darabi, R.; Akin, M.; Ayati, A.; Ayyildiz, S.; Bekmezci, M.; Bayat, R.; Fatih, S. Synthesis and characterization of activated carbon supported bimetallic Pd based nanoparticles and their sensor and antibacterial investigation. *Environ. Res.* **2023**, *221*, 115287. [[CrossRef](#)]
38. Sastry, M.; Mayya, K.S.; Bandyopadhyay, K. pH Dependent changes in the optical properties of carboxylic acid derivatized silver colloidal particles. *Colloids Surfaces A Physicochem. Eng. Asp.* **1997**, *127*, 221–228. [[CrossRef](#)]
39. Spoyală, A.; Ilie, C.I.; Dolete, G.; Petrișor, G.; Trușcă, R.D.; Motelica, L.; Ficai, D.; Ficai, A.; Oprea, O.C.; Dițu, M.L. The development of alginate/AgNPs/caffeic acid composite membranes as adsorbents for water purification. *Membranes* **2023**, *13*, 591. [[CrossRef](#)] [[PubMed](#)]
40. Kathiravan, V.; Ravi, S.; Ashokkumar, S.; Velmurugan, S.; Elumalai, K.; Khatiwada, C.P. Green synthesis of silver nanoparticles using *Croton sparsiflorus* morong leaf extract and their antibacterial and antifungal activities. *Spectrochim. Acta Part A Mol. Biomol. Spectrosc.* **2015**, *139*, 200–205. [[CrossRef](#)] [[PubMed](#)]
41. Kapoor, R.T. Biosynthesis and characterization of silver nanoparticles from *Croton bonplandianum* Baill and its antioxidant activity. *Int. J. Pharm. Res. Allied Sci.* **2015**, *4*, 39–44.
42. Ying, S.; Guan, Z.; Ofoegbu, P.C.; Clubb, P.; Rico, C.; He, F.; Hong, J. Green synthesis of nanoparticles: Current developments and limitations. *Environ. Technol. Innov.* **2022**, *26*, 102336. [[CrossRef](#)]
43. Oladotun, P.B.; Anuoluwa, A.A.; Adeyemi, A.O.; Williams, A.B.; Benson, N.U. Dataset on phytochemical screening, FTIR and GC-MS characterisation of *Azadirachta indica* and *Cymbopogon citratus* as reducing and stabilising agents for nanoparticles synthesis. *Data Br.* **2018**, *20*, 917–926.
44. Shaheen, G.; Ashfaq, A.; Khawar, A.; Jamil, Q.A.; Parveen, R.; Hadi, F.; Ghauri, O.; Shirazi, J.H.; Asif, H.M.; Shamin, T.; et al. Fourier transform infrared spectrometer analysis and antimicrobial screening of ethanolic extract of *Operculina terpathum* from cholistan desert. *Pharm. Pract.* **2022**, *20*, 2647.
45. Wongsu, P.; Phatikulrungsun, P.; Prathumthong, S. FT-IR characteristics, phenolic profiles and inhibitory potential against digestive enzymes of 25 herbal infusions. *Sci. Rep.* **2022**, *12*, 6631. [[CrossRef](#)]
46. Ganesan, V.; Deepa, B.; Nima, P.; Astalakshmi, A. Bio-inspired synthesis of silver nanoparticles using leaves of *Millingtonia hortensis*. *Int. J. Adv. Biotechnol. Res.* **2014**, *5*, 93–100.
47. Moteriya, P.; Chanda, S. Biosynthesis of silver nanoparticles formation from *Caesalpinia pulcherrima* stem metabolites and their broad spectrum biological activities. *J. Genet. Eng. Biotechnol.* **2018**, *16*, 105–113. [[CrossRef](#)]
48. Rahim, K.A.; Mahmoud, S.Y.; Ali, A.; Almaary, K.S.; Mustafa, A.B.Z.M.A.; Hussein, S.M. Extracellular biosynthesis of silver nanoparticles using *Rhizopus stolonifer*. *Saudi J. Biol. Sci.* **2017**, *24*, 208–216.
49. Odugu, A.N.; Daouda, K.; Keilah, L.P.; Tabi, G.A.; Rene, L.N.; Nsami, N.J.; Mbadcam, K.J. Effect of doping activated carbon based *Ricinodendron heudelottii* shells with AgNPs on the adsorption of indigo carmine and its antibacterial properties. *Arab. J. Chem.* **2020**, *13*, 5241–5253. [[CrossRef](#)]
50. Radičić, R.; Maletić, D.; Blažeka, D.; Car, J.; Krstulović, N. Synthesis of silver, gold, and platinum doped zinc oxide nanoparticles by pulsed laser ablation in water. *Nanomaterials* **2022**, *12*, 3484. [[CrossRef](#)] [[PubMed](#)]
51. Tensay, G.K.; Zenebe, T.M.; Ameha, K.; Chaithanya, K.K. Phytochemical screening and evaluation of antibacterial activities of *Croton macrostachyus* stem bark extracts. *Drug Invent Today* **2018**, *10*, 2727–2733.
52. Ali, R.; Aslam, Z.; Shawabkeh, R.A.; Asghar, A.; Hussein, I.A. BET, FTIR, and RAMAN characterizations of activated carbon from waste oil fly ash. *Turk. J. Chem.* **2020**, *44*, 279–295. [[CrossRef](#)] [[PubMed](#)]
53. Jaleh, B.; Fakhri, P. Chapter 5: Infrared and Fourier transform infrared spectroscopy for nanofillers and their nanocomposites. In *Spectroscopy of Polymer Nanocomposites*; William Andrew Publishing: Norwich, NY, USA, 2016; pp. 112–129.
54. Asey, M.N.; Esa, N.M.; Abdullah, C.A.C. Synthesis and characterization of magnetic nanoparticles (MNP) and MNP-chitosan composites. *Malaysian J. Sci. Tech.* **2019**, *4*, 39–44. [[CrossRef](#)]
55. Islam, M.N.; Khatton, A.; Sarker, J.; Sikder, H.A.; Chowdhury, A.M.S. Preparation and characterization of activated carbon from Jute stick by chemical activation: Comparison of different activating agents. *Saudi J. Eng. Technol.* **2022**, *7*, 112–117. [[CrossRef](#)]
56. Raut, E.R.; Thakur, M.A.B.; Chaudhari, A.R. Comparative study of preparation and characterization of activated carbon obtained from sugarcane bagasse and rice husk by using H₃PO₄ and ZnCl₂. *Mater. Today Proc.* **2022**, *66*, 1875–1884. [[CrossRef](#)]
57. Altammar, K.A. A review on nanoparticles: Characteristics, synthesis, applications, and challenges. *Front. Microbiol.* **2023**, *14*, 1155622. [[CrossRef](#)]
58. Ndi, N.J.; Ketcha, M.J.; Anagho, G.S.; Ghogomu, N.J.; Belibi, E. Physical and chemical characteristics of activated carbon prepared by pyrolysis of chemically treated cola nut (*Cola acuminata*) shells wastes and its ability to adsorb organics. *Int. J. Adv. Chem. Technol.* **2014**, *2014*, 2–4.
59. Pandey, P.; Karki, B.; Lekhak, B.; Koirala, A.R.; Sharma, R.K.; Pant, H.R. Comparative antibacterial study of silver nanoparticles doped activated carbon prepared by different methods. *J. Inst. Eng.* **2018**, *15*, 187–194. [[CrossRef](#)]
60. Abongta, M.L. Effect of Carbonization and Doping on the Antibacterial and Antioxidant Potentials of *Cola acuminata* Shells. Master's Thesis, University of Yaoundé I, Yaoundé, Cameroon, 2020.

61. Sánchez-López, E.; Gomes, D.; Esteruelas, G.; Bonilla, L.; Lopez-Machado, A.L.; Galindo, R.; Cano, A.; Espina, M.; Ettcheto, M.; Camins, A.; et al. Metal-based nanoparticles as antimicrobial agents: An overview. *Nanomaterials* **2020**, *10*, 292. [[CrossRef](#)] [[PubMed](#)]
62. Saiganesh, S.; Krishnan, T.; Narasimha, G.; Almoallim, H.S.; Alhari, S.A.; Reddy, L.V.; Mallikarjuna, K.; Mohammed, A.; Prabhakar, V.S.V. Phytosynthetic fabrication of lanthanum ion-doped nickel oxide nanoparticles using *Sesbania grandiflora* leaf extract and their anti-microbial properties. *Crystals* **2021**, *11*, 124. [[CrossRef](#)]
63. Hileuskaya, K.; Ladutska, A.; Kulikouskaya, V.; Kraskouski, A.; Novik, G.; Kozerozhets, I.; Kozlovskiy, A.; Agabekov, V. 'Green' approach for obtaining stable pectin-capped silver nanoparticles: Physico-chemical characterization and antibacterial activity. *Colloids Surf. A* **2020**, *585*, 124141. [[CrossRef](#)]
64. Chengzhu, L.; Yuchao, L.; Sie, C.T. Bactericidal and cytotoxic properties of silver nanoparticles. *Int. J. Mol. Sci.* **2019**, *20*, 449.
65. Ozdal, M.; Gurkok, S. Recent advances in nanoparticles as antibacterial agent. *Admet Dmpk* **2022**, *10*, 115–129. [[CrossRef](#)] [[PubMed](#)]
66. Zayed, M.F.; Mahfoze, R.A.; El-kousy, S.M.; Al-Ashkar, E.A. *In-vitro* antioxidant and antimicrobial activities of metal nanoparticles biosynthesized using optimized *Pimpinella anisum* extract. *Colloids Surf. A* **2020**, *585*, 124167. [[CrossRef](#)]
67. Jackson, T.; Patani, B.; Israel, M. Nanomaterials and cell interactions: A review. *J. Biomater. Nanobiotechnol.* **2017**, *8*, 220–228. [[CrossRef](#)]
68. Abarca-Cabrera, L.; Fraga-García, P.; Berensmeier, S. Bio-nano interactions: Binding proteins, polysaccharides, lipids and nucleic acids onto magnetic nanoparticles. *Biomater. Res.* **2021**, *25*, 12. [[CrossRef](#)]
69. Basavegowda, N.; Baek, K.H. Multimetallic nanoparticles as alternative antimicrobial agents: Challenges and perspectives. *Molecules* **2021**, *26*, 912. [[CrossRef](#)]
70. Mbekou, I.K.; Dize, D.; Yimgang, V.L.; Djague, F.; Toghueo, R.M.K.; Norbert, S.; Lenta, B.N.; Boyom, F.F. Antibacterial and mode of action of extracts from endophytic fungi derived from *Terminalia mantaly*, *Terminalia catappa*, and *Cananga odorata*. *Biomed. Res. Int.* **2021**, *2021*, 6697973. [[CrossRef](#)] [[PubMed](#)]
71. Whittaker, J.W. Non-heme manganese catalase—the “other” catalase. *Arch. Biochem. Biophys.* **2012**, *525*, 111–120. [[CrossRef](#)] [[PubMed](#)]
72. Yuan, F.; Yin, S.; Xu, Y.; Xiang, L.; Wang, H.; Li, Z.; Fan, K.; Pan, G. The richness and diversity of catalases in bacteria. *Front. Microbiol.* **2021**, *12*, 645477. [[CrossRef](#)] [[PubMed](#)]
73. Nasehir, K.E.M.; Yahaya, M.F.; Ismail, A.; Mohd, A.A. Effect of preparation conditions of activated carbon prepared from rice husk by ZnCl₂ activation for removal of Cu (II) from aqueous solution. *Int. J. Eng. Technol.* **2010**, *10*, 27–32.
74. Cockerill, F.R., III; Wikler, M.A.; Alder, J.; Dudley, M.N.; Eliopoulos, G.M.; Ferraro, M.J.; Hardy, D.J.; Hecht, D.W. *Methods for Dilution Antimicrobial Susceptibility Tests for Bacteria That Grow Aerobically*, 9th ed.; Clinical Laboratory Standard Institute: Berwyn, PA, USA, 2012; Volume 29.
75. Bowling, T.; Mercer, L.; Don, R.; Jacobs, R.; Nare, B. Drugs and drug resistance application of a resazurin-based high-throughput screening assay for the identification and progression of new treatments for human African trypanosomiasis. *Int. J. Parasitol. Drugs Drug Resist.* **2012**, *2*, 262–270. [[CrossRef](#)]
76. Nguimatsia, F.; Kenmogne, S.B.; Ngo-Mback, M.N.; Kouamouo, J.; Tchuitio, N.L.; Melogmo, D.Y.; Dongmo, J.P.M. Antibacterial activities of the essential oil and hydroethanolic extract from *Aeollanthus heliotropioides* Oliv. *Mediterr. J. Chem.* **2021**, *97*, 2021.
77. Carson, C.F.; Mee, B.J.; Riley, T.V. Mechanism of action of *Melaleuca alternifolia* (tea tree) oil on *Staphylococcus aureus* determined by time-kill, lysis, leakage, and salt tolerance assays and electron microscopy *Antimicrob. Agents Chemother.* **2002**, *46*, 1914–1920. [[CrossRef](#)]

Disclaimer/Publisher's Note: The statements, opinions and data contained in all publications are solely those of the individual author(s) and contributor(s) and not of MDPI and/or the editor(s). MDPI and/or the editor(s) disclaim responsibility for any injury to people or property resulting from any ideas, methods, instructions or products referred to in the content.